Applied Physics Letters

PERSPECTIVE | FEBRUARY 20 2024

Perspectives and progress on wurtzite ferroelectrics: Synthesis, characterization, theory, and device applications

Joseph Casamento ; Steven M. Baksa ; Drew Behrendt ; Sebastian Calderon ; Devin Goodling; John Hayden ; Fan He ; Leonard Jacques ; Seung Hoon Lee ; Walter Smith ; Albert Suceava ; Quyen Tran ; Xiaojun Zheng ; Rui Zu ; Thomas Beechem ; Ismaila Dabo ; Elizabeth C. Dickey ; Giovanni Esteves ; Venkatraman Gopalan ; Michael David Henry ; Jon F. Ihlefeld ; Thomas N. Jackson; Sergei V. Kalinin ; Kyle P. Kelley ; Yongtao Liu ; Andrew M. Rappe ; Joan Redwing ; Susan Trolier-McKinstry ; Jon-Paul Maria

Appl. Phys. Lett. 124, 080501 (2024)
https://doi.org/10.1063/5.0185066

AIP Publishing

Perspectives and progress on wurtzite ferroelectrics: Synthesis, characterization, theory, and device applications

Cite as: Appl. Phys. Lett. **124**, 080501 (2024); doi: 10.1063/5.0185066
Submitted: 28 October 2023 · Accepted: 18 December 2023 ·
Published Online: 20 February 2024

Joseph Casamento,[1,a)] Steven M. Baksa,[1] Drew Behrendt,[2] Sebastian Calderon,[3] Devin Goodling,[1] John Hayden,[1] Fan He,[1] Leonard Jacques,[4] Seung Hoon Lee,[1] Walter Smith,[5] Albert Suceava,[1] Quyen Tran,[1] Xiaojun Zheng,[1] Rui Zu,[1] Thomas Beechem,[5] Ismaila Dabo,[1] Elizabeth C. Dickey,[3] Giovanni Esteves,[6] Venkatraman Gopalan,[1] Michael David Henry,[6] Jon F. Ihlefeld,[7] Thomas N. Jackson,[1] Sergei V. Kalinin,[8] Kyle P. Kelley,[9] Yongtao Liu,[9] Andrew M. Rappe,[2] Joan Redwing,[1] Susan Trolier-McKinstry,[1] and Jon-Paul Maria[1]

AFFILIATIONS

[1]Department of Materials Science and Engineering and Materials Research Institute, Pennsylvania State University, University Park, Pennsylvania 16802, USA
[2]Department of Chemistry, University of Pennsylvania, Philadelphia, Pennsylvania 19104, USA
[3]Department of Materials Science and Engineering, Carnegie Mellon University, Pittsburgh, Pennsylvania 15213, USA
[4]Department of Engineering Science and Mechanics and Materials Research Institute, Pennsylvania State University University Park, Pennsylvania 16802, USA
[5]School of Mechanical Engineering and Birck Nanotechnology Center, Purdue University, Lafayette, Indiana 47907, USA
[6]Microsystems Engineering, Science and Applications, Sandia National Laboratories, Albuquerque, New Mexico 87123, USA
[7]Department of Materials Science and Engineering, University of Virginia, Charlottesville, Virginia 22904, USA
[8]Materials Science and Engineering Department, University of Tennessee, Knoxville, Knoxville, Tennessee 37916, USA
[9]Center for Nanophase Materials Sciences, Oak Ridge National Laboratory, Oak Ridge, Tennessee 37830, USA

[a)]**Author to whom correspondence should be addressed:** jac5956@psu.edu

ABSTRACT

Wurtzite ferroelectrics are an emerging material class that expands the functionality and application space of wide bandgap semiconductors. Promising physical properties of binary wurtzite semiconductors include a large, reorientable spontaneous polarization, direct band gaps that span from the infrared to ultraviolet, large thermal conductivities and acoustic wave velocities, high mobility electron and hole channels, and low optical losses. The ability to reverse the polarization in ternary wurtzite semiconductors at room temperature enables memory and analog type functionality and quasi-phase matching in optical devices and boosts the ecosystem of wurtzite semiconductors, provided the appropriate combination of properties can be achieved for any given application. In this article, advances in the design, synthesis, and characterization of wurtzite ferroelectric materials and devices are discussed. Highlights include: the direct and quantitative observation of polarization reversal of $\sim$135 μC/cm^2 charge in $Al_{1-x}B_xN$ via electron microscopy, $Al_{1-x}B_xN$ ferroelectric domain patterns poled down to 400 nm in width via scanning probe microscopy, and full polarization retention after over 1000 h of 200 °C baking and a 2× enhancement relative to ZnO in the nonlinear optical response of $Zn_{1-x}Mg_xO$. The main tradeoffs, challenges, and opportunities in thin film deposition, heterostructure design and characterization, and device fabrication are overviewed.

I. INTRODUCTION

Wurtzite semiconductors, including zinc oxide (ZnO) and aluminum nitride (AlN), gallium nitride (GaN), indium nitride (InN), and their alloys, are critical components of numerous electronic, photonic, and acoustic systems. These systems span a wide voltage and frequency range and include photodetectors, light emitting diodes, lasers, transistors, and bulk and surface acoustic wave resonators.[1–5] The impact of these technologies is further enhanced by the fact that wurtzite

semiconductors are the leading candidates for high temperature, harsh environment electronics. Consequently, their monolithic integration efforts with silicon complementary metal–oxide–semiconductor (CMOS) integrated circuits have increased in recent years to improve on-chip power delivery and switching speeds. For example, epitaxial GaN integration on 300 mm diameter silicon wafers has been demonstrated, providing monolithic integration opportunities for GaN based technologies such as compact millimeter wave and radio frequency (RF) integrated circuits.[6,7]

The technological relevance of wurtzite semiconductors is a result of strong metal-anion bonds, direct bandgaps from the infrared to ultraviolet, and tunable lattice parameters from cation alloying [e.g., aluminum indium nitride ($Al_{1-x}In_xN$)]. However, the physical property that most distinguishes wurtzites from other technologically relevant semiconductors is the spontaneous polarization that arises in the wurtzite unit cell along the crystallographic *c* axis. Unlike silicon and gallium arsenide (GaAs) based heterostructures, chemical doping is not needed to generate mobile charge carriers in polar nitride heterostructures. Heterojunction polarization discontinuities lead to confined electron channels [e.g., two-dimensional electron gases (2DEGs)][8–10] with high mobility and more recently hole channels.[11] These channels serve as the backbone of nitride high electron mobility transistors (HEMTs), for power amplifiers in RF integrated circuits. All of these aspects allow nitrides in devices with high operational temperatures, efficient light emission and low optical losses, strong electromechanical coupling, high breakdown voltage, and ultrahigh frequency operation.

For more than one century, wurtzite crystals were understood to be piezoelectric and pyroelectric, but not ferroelectric. Namely, dielectric breakdown was expected (and observed) before field-induced polarization reversal because the energy barrier was too large. However, alloying approaches were discovered in the late 2000s that boosted the piezoelectric response of AlN by nearly 4X through Sc substitution for Al.[12] In 2019, it was shown that the high-Sc content aluminum scandium nitride ($Al_{1-x}Sc_xN$) alloys were also ferroelectric.[13] A similar notion for distorting the bonding environment to lower the energy barrier for polarization reversal was manifest in aluminum boron nitride ($Al_{1-x}B_xN$), where boron nitride (BN) itself is stable in the layered hexagonal phase, which was predicted to be the transient, intermediate crystal structure in polarization reversal for ferroelectric wurtzites.[14] Accordingly, ferroelectricity was experimentally observed in newer wurtzite ternary alloys such as $Al_{1-x}B_xN$[15] and zinc magnesium oxide ($Zn_{1-x}Mg_xO$) in 2021.[16]

The ability to engineer ferroelectricity and nonlinear property responses in the wurtzite crystal structure comes with distinct technological advantages, if structure–property relationships and associated tradeoffs in processing and physical properties are established. For example, $Al_{1-x}Sc_xN$ boasts ferroelectricity and enhanced piezoelectric, dielectric, and non-linear optical responses,[17–21] but the quality factor at resonance in acoustic devices is degraded in part due to the ionic nature of the scandium–nitrogen bond. In addition, the thermal conductivity decreases and optical losses of AlN increase when alloyed with scandium.[21,22] These examples highlight significant opportunities to engineer and improve desired physical properties in wurtzite ferroelectrics and tailor their application space. These potential opportunities include, but are not limited to, the design of new materials that accommodate symmetry mismatched constituent compounds, synthesis strategies that facilitate formation of thermodynamically metastable phases, characterization techniques that analyze these materials in extreme conditions, and new device designs that incorporate these new physical properties.

This perspective discusses recent advancements in wurtzite ferroelectric materials, with a focus on $Al_{1-x}B_xN$ and $Zn_{1-x}Mg_xO$ and a comparison to $Al_{1-x}Sc_xN$ highlighting commonalities and differences. Progress in the synthesis, theory and design, characterization, and device fabrication of wurtzite ferroelectrics is presented. This perspective also provides a broad overview of applications for wurtzite ferroelectrics and an outlook on integrating their desired physical properties into next generation electronic, photonic, and acoustic technologies. While perspective articles involving wurtzite ferroelectrics have been written recently[23,24] this perspective differs by providing insight into challenges and opportunities for understanding and reducing leakage current densities at large electric fields; from synthesis via physical vapor deposition (PVD) to metal–organic chemical vapor deposition (MOCVD) and complementary characterization methods such as scanning transmission electron microscopy (STEM). It also discusses how those challenges and opportunities are linked to new devices that could leverage this emergent ferroelectric behavior.

II. THIN FILM DEPOSITION

$Al_{1-x}Sc_xN$ was the first experimentally demonstrated ferroelectric nitride material in 2019; the films were deposited by reactive magnetron sputtering. A key feature to unveiling the ferroelectric behavior was the ability to reduce leakage current densities at electric fields above 3–5 MV/cm and reduce the coercive field below the breakdown field in this range. Since 2019, sputtering has become a popular technique to explore new ferroelectric wurtzites due to the ability to tailor energetics and generate insulating nitride compounds in a cost-effective, scalable deposition platform. Changes to adatom kinetic energy allow for engineering of point defect densities and microstructure, which in turn affect film stoichiometry and electrical resistivity. Wurtzite ferroelectrics have been predicated on alloying the binary semiconductors of AlN and ZnO on the cation sites to induce distortions in local bonding environments, pushing the system toward a crystallographic phase transformation to facilitate polarization reversal. Many such alloys are metastable in nature, which favors deposition techniques that proceed out of equilibrium to kinetically stabilize these materials. For example, Mg alloyed ZnO has a thermodynamic solubility limit of ~22% Mg[25] in the wurtzite structure at the eutectic point near 1800 °C and the solubility decreases significantly with decreasing temperature. Nevertheless, sputtered $Zn_{1-x}Mg_xO$ alloys deposited at room temperature have achieved upward of 37% Mg in the wurtzite structure. Tailored energetics, tuned synthesis parameters, and low substrate temperatures can extend solubility limits well into metastable composition space. This extends to plasma assisted molecular beam epitaxy (MBE), a growth technique which also utilizes moderate growth temperatures with a remote plasma, which has been utilized to generate ferroelectric nitrides.[26–28]

Sputtering and MBE are not the most commonly utilized deposition techniques for active semiconductor device layers in the semiconductor industry. MOCVD and a subset of MOCVD, atomic layer deposition (ALD), are utilized due to cost-effectiveness when depositing on 300 mm substrates and conformal deposition. For integrating a memory layer directly on a logic transistor, the space around fin field effect transistors (FinFETs) and future nanoribbon FETs is very limited (~2 nm) and requires conformal deposition. Hence, ALD and/or CVD will be the ultimate deposition technique for that specific

application. While there are no known demonstrations of ferroelectricity in CVD and ALD-prepared wurtzites to date, the parent compounds of AlN and ZnO have been investigated and compositions including those that have been shown to be ferroelectric when grown by other techniques. For example, plasma-enhanced ALD processes exist for synthesis of both polycrystalline[29,30] and epitaxial AlN.[31] There are also reports of ALD-prepared AlN films that are strongly (0001) oriented, with respectable piezoelectric coefficients, low carbon and oxygen impurity levels, and low leakage under fields approaching 8 MV/cm, which suggests that through process development, ferroelectric AlN-based wurtzites are feasible.[32] In addition, significant recent advancements have been made in CVD deposition of $Al_{1-x}Sc_xN$ and $Al_{1-x}Y_xN$ alloys, involving new precursor development and utilization of precursors used in ALD half reactions.[33–36] Future work involving high purity precursor development with higher vapor pressures will be crucial to expedited progress. The high temperature, plasma-free growth of CVD presents unique opportunities and challenges for synthesis of metastable materials like $Al_{1-x}Sc_xN$. The ability to understand processing–property relationships and engineer microstructure and defect formation and prevent phase separation across all deposition techniques from PVD to CVD will enable the largest opportunities for heterostructure design, targeted applications, and technological implementation for nitride ferroelectrics. Figure 1 shows a general landscape of temperature-energy space for the synthesis techniques commonly utilized for wurtzite semiconductors.

III. ELECTRON MICROSCOPY

To guide synthesis routes of the expanding wurtzite ferroelectric family, STEM and the corresponding elemental distribution by energy dispersive spectroscopy (EDS) offer the ability to observe structural and chemical changes at atomic resolution. These techniques build on recent advances in the field of electron microscopy and serve as key methods

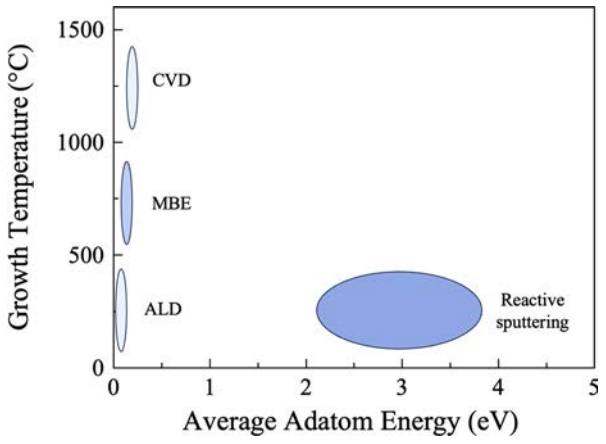

FIG. 1. Typical growth temperatures for wurtzite semiconductors vs average adatom energy for various deposition techniques. These numbers do not take into account tailored processes (e.g., thermalization in high-pressure sputtering which lowers average energy or the plasma electron temperature in plasma-assisted MBE), the Maxwellian vs Gaussian energy distribution differences, and other factors such as strain and chemical potentials that affect the overall ability to obtain wurtzite films with *c*-axis orientation. For MBE, CVD, and ALD techniques, the principal adatom energy is thermal (k_bT) and in sputtering, it is due to the kinetic energy of ejected atoms from the cathode.

to understanding the structure–property relationship in wurtzite ferroelectrics. STEM has been extensively used to characterize wurtzite materials, providing information about inversion domain boundaries (IDB), interphases, strain, phase identification, and defects,[37–42] [see Fig. 2(a)]. After ferroelectricity was first experimentally demonstrated in $Al_{1-x}Sc_xN$,[13] (S)TEM studies of wurtzite ferroelectrics have been primarily focused on determining the effect of the dopants such as Sc and B in AlN and Mg in ZnO on the local structural characteristics. Investigating grain growth and texture,[43–48] phase separation and distributions,[49–52] strain,[53] and interfaces[54] have helped identify proper deposition conditions to produce uniform *c*-axis textured films, avoid dopant segregation, and identify phase inhomogeneities and phase separation that can be detrimental to the ferroelectric properties. For example, a detailed study of the abnormal grain growth as a function of Sc content[55] in magnetron sputtered $Al_{1-x}Sc_xN$ ($x = 0–0.43$) demonstrated the segregation of Sc to the columnar grain boundaries [see Fig. 2(b)]. This showed that abnormally oriented grains (AOGs) do not nucleate at the substrate interface and provided insight into how certain deposition parameters may promote AOG formation.

Furthermore, STEM capabilities can be extended to study ferroelectric domain distributions, domain boundaries, polarization, and switching mechanisms at the nanoscale. Moreover, the local spontaneous polarization, at the unit-cell scale level, can be mapped and quantified[56] by locating the atomic columns and applying the modern theory of polarization.[57,58] Polarization values can even be obtained for binary wurtzite structures, such as AlN,[59] where ferroelectric switching was previously inaccessible due to the material dielectric breakdown.[60] This is extremely timely as the measured remanent polarization values for wurtzites are in general agreement with those from first principles calculations following the modern theory of polarization and utilizing the nonpolar layered hexagonal structure as in Ref. 61.

In $Al_{0.94}B_{0.06}N$, studies have demonstrated a good agreement between the calculated structure-based polarization via STEM (140 ± 14 μC cm^{-2}) and the remanent polarization (138 ± 1 μC cm^{-2}) measured via hysteresis loops,[59] where a vector map for individual unit-cell polarization can be attained [see Fig. 2(c)]. General characterization of the polarization direction can be also obtained by observing the structure along the [110] zone axis. For example, atomic resolution annular bright field (ABF) STEM was utilized to show that sputter deposited $Al_{1-x}Sc_xN$ changes from metal polar orientation to nitrogen polar after 40 nm thickness when grown on metal polar GaN substrates, indicating the propensity for sputter deposited films to adopt a nitrogen polar orientation.[53] Qualitative polarization mapping for large fields of view at low magnification[54] is also feasible, by exploiting a preferential electron scattering along the polar direction in ferroelectric materials, arising from dynamical scattering, which breaks Friedel's laws. These methodologies have been used to determine local polarization after *ex situ* electrical switching experiments[59,62] [see Fig. 2(d)] and may be further applied to evaluate the role of defects, elemental segregation, and interphases on the local polarization. It should be noted, however, that sample preparation techniques should be identified which do not alter the polarization, as can occur during focused-ion-beam preparation. Furthermore, careful consideration of the experimental conditions is necessary to disentangle polarization response, sample thickness, and sample tilts.[21,63]

Switching in wurtzite ferroelectrics occurs as domains toggle between a local metal- or anion-polar state. In the case of $Al_{1-x}B_xN$,

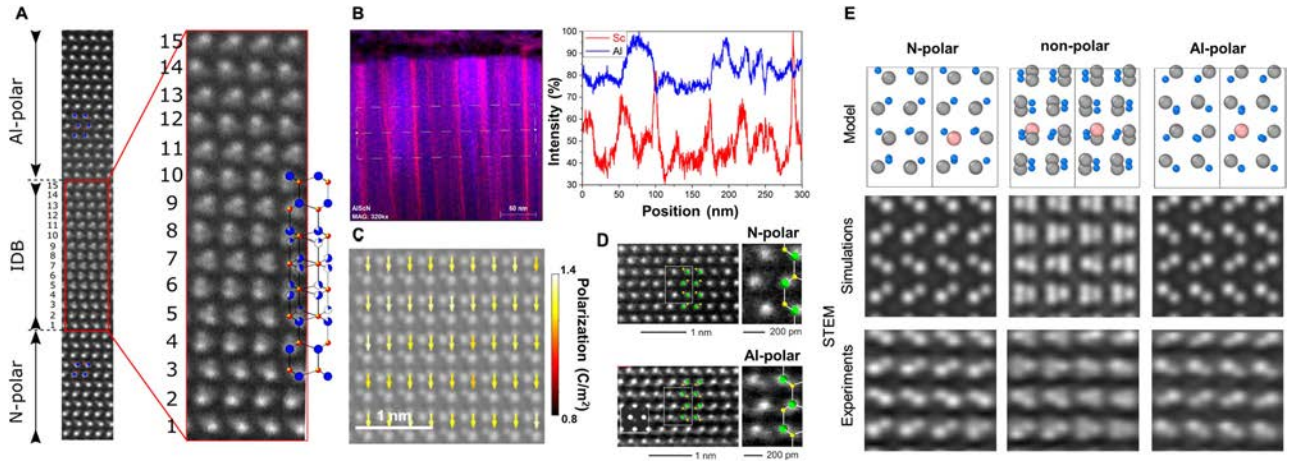

FIG. 2. (a) ADF-STEM image of an inversion domain boundary (IDB) between an N-polar domain and Al-polar in AlN. Adapted from Stolyarchuk *et al.*, Sci. Rep. **8**, 14111 (2018). Copyright 2018 Author(s), licensed under a Creative Commons Attribution (CC BY) license.[39] (b) STEM-EDS maps on 10% Sc film showing Sc enrichment at the grain boundary in the intensity profiles (right). Reproduced with permission from Sandu *et al.*, Phys. Status Solidi A **216**, 1800569 (2019). Copyright 2023 John Wiley and Sons.[55] (C) Differentiated differential phase contrast (dDPC)-STEM image of $Al_{0.94}B_{0.06}N$ overlapped with a polarization vector map at each unit cell. Reproduced with permission from Calderon *et al.*, Science **380**, 1034 (2023). Copyright 2023 The American Association for the Advancement of Science (AAAS).[59] (D) Annular dark field (ADF)-STEM images for N-polar atomic structure in the as-deposited $Al_{1-x}Sc_xN$ and Al-polar atomic structure in the switched $Al_{1-x}Sc_xN$, the polarization inversion is attained *ex situ*. Reproduced with permission from Wolff *et al.*, J. Appl. Phys. **129**, 034103 (2021). Copyright 2021 AIP Publishing LLC.[62] (e) Atomic models, STEM image simulations, and experimental images for the N-polar, nonpolar, and Al-polar in $Al_{0.94}B_{0.06}N$ occurring during a switching event. Reproduced with permission from Calderon *et al.* Science **380**, 1034 (2023). Copyright 2023 The American Association for the Advancement of Science (AAAS).[59]

this is in response to aluminum/boron nitride rings "puckering" in one direction or another.[59] With this toggling of the polar state, ferroelectric domain walls in wurtzite materials have a structure analogous to the inversion domains long studied in these materials,[64–67] but in some cases also have a horizontal component,[68] which poses significant opportunities to investigate the possibility of charged domain walls in wurtzite ferroelectrics. *In situ* biasing experiments in ferroelectrics are commonly utilized to study dynamic processes using *in situ* bias holders in the TEM;[69] however, in wurtzite ferroelectrics, these studies have been hindered by the high electric fields required to switch the polarization. Electrode migration and/or electrode grain growth for such thin specimens breakdown the samples before the polarization reversal is attained. To avoid this limitation, electron beam-induced charging has been utilized as an alternative method to observe *in situ* switching pathways in $Al_{0.94}B_{0.06}N$,[59] which enabled the identification of a transient antipolar phase. This antipolar phase has a β-BeO-like structure, as predicted by density functional theory (DFT) calculations,[59,70] indicating a sequential switching mechanism as shown in Fig. 2(e).

Although a significant body of literature exists for $Al_{1-x}Sc_xN$, other wurtzite ferroelectrics, such as $Al_{1-x}B_xN$ and $Zn_{1-x}Mg_xO$, need to be systematically explored. In addition, significant efforts need to be placed in identifying switching mechanisms for a variety of compositions, as well as characterizing the electrode interface region to better understand the local structure evolution during polarization inversion. Additional strategies need to be designed to characterize the effect of local distortion, defects, and bonding states at the electrode interfaces on the switching mechanisms and wake-up processes in wurtzite ferroelectrics, taking advantage of the picometer resolution that can be achieved in modern STEM instrumentation.

IV. SCANNING PROBE MICROSCOPY, LOCAL PROBES

A characteristic feature of ferroelectric materials is the formation of ferroelectric domain structures, which form to minimize depolarization fields and accommodate strain fields and disorder[71] (e.g., ions, adsorbates, planar defects, and grain boundaries). Ferroelectric domain dynamics are directly connected to the fundamental physics of ferroelectric materials, namely, the nature of the order parameter that governs ferroelectric behavior. A breakthrough in understanding the static and dynamic properties of domain structures in ferroelectric materials arrived with the invention of piezoresponse force microscopy (PFM), a subset of atomic force microscopy (AFM).[72,73] In PFM, the application of electrical bias to a conductive scanning probe microscopy tip results in an electromechanical strain, and consequently a surface deformation. Here, the surface deformation is directly detected via a laser reflected from an AFM tip. Similarly, the application of constant bias to the probe can be used to modify domain structures and explore phenomena such as domain nucleation and wall motion with nanometer scale resolution. Furthermore, DC bias sweeps with concurrent PFM detection yield the local electromechanical hysteresis loop that, on a qualitative level, can be interpreted similarly to macroscopic P-E loops.[74]

For the last two decades, PFM has been utilized to study piezoelectric nitride semiconductors such as AlN. Previously, nitride semiconductors were believed to be non-ferroelectric, and the PFM contrast observed in these materials was attributed to regions with metal and nitrogen polar surface terminations, respectively.[75] Since the discovery of ferroelectricity in nitrides, several authors have reported PFM measurements of local piezoelectric properties and grain-related polarization patterns.

The recent emergence of wurtzite ferroelectrics and the early demonstration of phenomena, such as wake up,[76] have opened questions regarding the spatially heterogeneous nanoscale mechanisms and domain dynamics associated with local polarization switching. Due to the relatively short history of ferroelectric wurtzites, few studies characterizing the local ferroelectric structure have been reported. As an example, ferroelectric switching is clearly shown in $Al_{0.94}B_{0.06}N$ *and* $Zn_{0.64}Mg_{0.36}O$ thin films. Figures 3(a) and 3(b) show post +60 V/−60 V DC poling band excitation PFM amplitude and phase images, respectively, for 150 nm thick $Zn_{0.64}Mg_{0.36}O$. Briefly, band excitation PFM uses a non-sinusoidal signal with a defined band in frequency space to independently detect the resonance frequency and response amplitude to mitigate topographic crosstalk. Here, clear remanent polarization switching is observed as indicated by written domain patterns and 180° phase switching. Similarly, Figs. 3(e) and 3(f) show post +15 V/−15 V poling with band excitation for 20 nm thick $Al_{0.94}B_{0.06}N$ with signatures of polarization reversal.

It is important to note that an important aspect of polarization switching from air-exposed surfaces in ferroelectric wurtzites is the possible coupling to surface electrochemical phenomena. Previously, such dynamics were discovered in the well-studied $LaAlO_3$-$SrTiO_3$ (LAO-STO) system, in which ionic screening of the polarization charge by hydroxides and protons (water reduction cycle) is a necessary component of the polarization switching in the LAO layer.[77,78] It is argued that similar behavior can be present on wurtzite surfaces, in which the surface termination changes upon polarization switching. Large voltages needed to switch the polarization can enhance surface electrochemistry effects when measured in ambient environments, which necessitates additional techniques to further evaluate polarization reversal pathways, domain wall motion, and the defects associated with the process.

V. OPTICAL PROPERTIES

A. Photoluminescence

As previously stated, some wurtzite domain walls have a structure analogous to the inversion domain boundaries that are also observed in the absence of ferroelectric behavior. Inversion domain boundaries in AlN have been linked to structural changes associated with the formation of Al–O bonds and intentional oxygen exposure during growth[79,80] (e.g., when the polarity inverts at an interface due to oxygen accumulation). Strong photoluminescence (PL) occurs at inversion boundaries in III–V semiconductors due to both the localized electric fields limiting non-radiative recombination and the defects that tend to cluster there.[66,67] By extension, PL offers a path to monitor domain wall motion while also providing a probe of defect evolution during switching. However, domains are typically smaller than the diffraction limit of standard optical characterization techniques. For this reason, PL will likely find its most widespread usage as a tool to understand defect evolution throughout device lifetime. Photoluminescence probes electronic states in a material by quantifying the emission of light as charge relaxes back to equilibrium after photoexcitation, and is well established in its ability to identify and differentiate defects in wurtzite materials.[81,82] Defects, meanwhile, have been suggested as a factor limiting the endurance of wurtzite ferroelectrics. For example, increased leakage currents in $Al_{1-x}Sc_xN$ devices have been attributed to positively charged defect accumulation near the contacts.[45,83,84] While positively charged defects reducing the Schottky barrier height are consistent with the measured increase in leakage current, direct experimental examination of the defect states evolving with switching is lacking.

With this motivation, the evolution of photoluminescence was examined as $Al_{0.93}B_{0.07}N$ metal-ferroelectric metal capacitors went

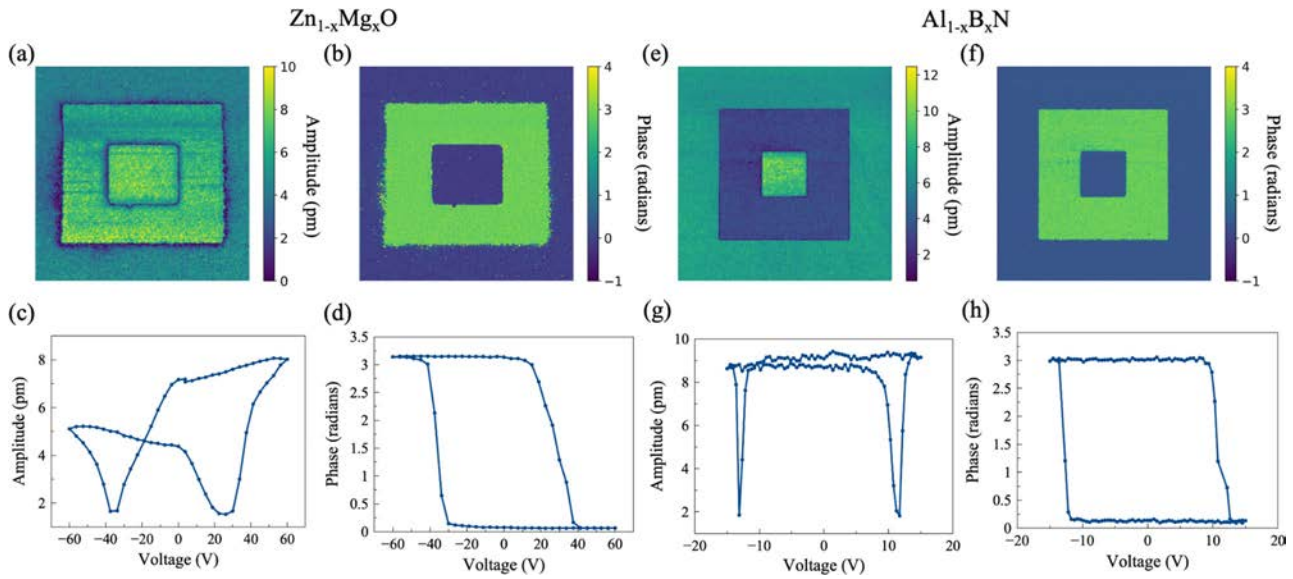

FIG. 3. Band excitation PFM of $Zn_{1-x}Mg_xO$ [(a)–(d)] and $Al_{1-x}B_xN$ films [(e)–(h)] showing piezoresponse amplitude and phase changes as a result of polarization reversal. Amplitude changes are linked to electromechanical changes that occur in the vicinity of adjacent domains, in this case a poled region. A uniform amplitude across a poled region with a difference in magnitude in an oppositely poled region is attributed to a finite electrostatic contribution. Polarization reversal from the nitrogen polar to metal polar state causes a phase shift of 180° (π radians). Here, square domain patterns are written by applying opposite polarity DC biases. The phase-voltage loops resemble polarization-voltage loops in electrical measurements. The measurements were performed in ambient for $Zn_{1-x}Mg_xO$ and in a glovebox environment for $Al_{1-x}B_xN$.

through wake-up. Wake-up was performed utilizing a procedure similar to that of Ref. 76 after which the top metal contacts were removed allowing for photoluminescence of the underlying $Al_{0.93}B_{0.07}N$. Systematic changes are observed in the photoluminescence shape and intensity in the 1.7–2.7 eV energy range (see Fig. 4). Specifically, PL-intensity decreases with wake-up even as the spectral signal near 1.8 eV increases relative to that near 2.2 eV. These sub-bandgap modes are located at energies typically associated with oxygen defect complexes, suggesting that these complexes are being modified by the wake-up process.[82,85] Future work will center on definitively assigning these features and assessing the implications on ferroelectric behavior and leakage currents. PL, as a nondestructive measurement technique, provides a means of efficiently monitoring defect contributions to the switching of wurtzite ferroelectrics through the depth of the heterostructure.

B. Second harmonic generation

Historically, the interest in III–V semiconductors originated from robust linear optical properties. For example, the technological driving force for development of GaN based electronic devices increased after efficient p type doping of Mg in GaN was discovered in the early 1990s; this enabled blue laser diodes and LEDs and the commercialization of white LEDs.[86–89] AlN, GaN, and their alloys provided the ability to tune lattice parameters and linear optical properties such as direct bandgaps and refractive indices in the ultraviolet regime through epitaxial growth, but the nonlinear optical applications remained little unexplored due to the relatively small nonlinear coefficients compared to materials like $LiNbO_3$.[90–92] This precluded their extensive use in additional applications in the fields of nanophotonics, biological imaging, telecommunications, and quantum computing. Alloying with Sc increases the second order non-linear optical coefficients of AlN by an order of magnitude, opening up opportunities in this design space. The combination of appreciable non-linear optical coefficients and optical transparency into the deep UV range due to the ultrawide bandgap gives $Al_{1-x}Sc_xN$ a distinct advantage vs other materials. Now

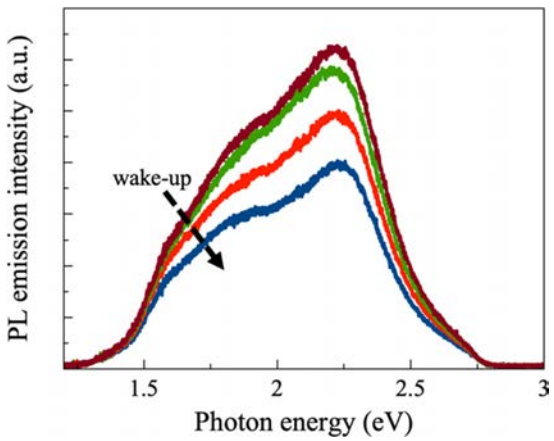

FIG. 4. Photoluminescence of $Al_{0.93}B_{0.07}N$ using a 405 nm wavelength excitation acquired at varying degrees of wake-up, with a decreasing intensity for increasing number of electrical measurement cycles. This change in the PL response is indicative of defect evolution and a change of defect concentrations during multiple measurements of polarization reversal cycles.

combined with the ability to achieve quasi-phase matching through periodic poling from polarization reversal, ferroelectric wurtzites are uniquely positioned for new photonic device architectures such as mirrorless optical parametric oscillators. The wide transparency range of ferroelectric wurtzites also promotes broadband photonic functionalities, such as Kerr comb generation, which utilizes third order ($\chi^{(3)}_{zzz}$) harmonic effects.[93] In $Al_{1-x}Sc_xN$, a maximum value of $d_{33} = \chi^{(2)}_{zzz} = 62.3 \pm 5.6$ pm/V at 1550 nm for 36% Sc content was reported,[21] roughly twice that of $LiNbO_3$, the most common material studied for CMOS compatible nonlinear optical systems. Recently, quasi-phase matching (QPM) has been explored in 200 nm thick $Al_{1-x}Sc_xN$ with periodic poling to generate domain widths of approximately 220 nm for a periodicity of 440 nm.[94] This gives significant promise to generating even smaller feature sizes with extreme ultraviolet (EUV) lithographic processes utilized in advanced technology nodes. More importantly, wurtzite nitrides like $Al_{1-x}Sc_xN$ can be grown directly on Si without heterogeneous integration, unlike $LiNbO_3$. Currently, commercially produced $LiNbO_3$ with low optical and acoustic losses is ion sliced and wafer bonded to integrate on Si.[95,96]

The enhancement of nonlinear optical coefficients in $Al_{1-x}B_xN$ with x is less pronounced compared to $Al_{1-x}Sc_xN$, as shown in Fig. 5(b) with the largest coefficient, d_{33}, remaining effectively unchanged, while an enhancement of d_{31} and d_{15} was observed. Maximum values of $d_{33} = 10.7 \pm 1.4$ pm/V, $d_{31} = 0.9 \pm 0.1$ pm/V, and $d_{15} = 1.2 \pm 0.07$ pm/V at 800 nm were measured via second harmonic generation (SHG) at 11% B content. Figure 5(c) demonstrates a quasi-phase matched structure with domains 400 nm in length prepared through poling with a biased AFM tip in PFM measurements.[97] In $Zn_{1-x}Mg_xO$, a complex relationship between Mg content and nonlinear susceptibilities was observed. A maximum enhanced value of $d_{33} = 10.1 \pm 2.7$ was reported with 23% Mg content, almost 50% greater than single crystal ZnO.[98] In addition, the electro-optic properties have been reported, with an effective Pockels coefficient of 7.6 ± 0.2 pm/V in films with 28% Mg content, a threefold enhancement over previously reported ZnO films.[99] The difference in non-linear optical properties between $Zn_{1-x}Mg_xO$, $Al_{1-x}Sc_xN$, and $Al_{1-x}B_xN$ points toward lattice and electron anharmonicity being key factors for tailoring non-linear optical responses in wurtzite ferroelectrics.

VI. ELECTRICAL PROPERTIES

The ultrawide bandgaps of wurtzite ferroelectrics arise, in part, from strong interatomic bonds in the crystals. This has important implications on the electrical characteristics of these materials. There are now several homologues of ferroelectric wurtzite compounds, including $Al_{1-x}Sc_xN$, $Al_{1-x}B_xN$, $Al_{1-x}Y_xN$,[28] $Ga_{1-x}Sc_xN$,[100] and $Zn_{1-x}Mg_xO$, and it is likely that the richness of the composition space will continue to grow. These compounds show large, electrically reversible polarizations (typically with remanent polarizations from 80 to 130 $\mu C/cm^2$), and bandgaps from 3 to 6.2 eV. Figure 6 compares the measured polarization—electric field hysteresis loops of important ferroelectric materials, including several of the wurtzite-structured ferroelectrics with $PbZr_{1-x}Ti_xO_3$ and $Hf_{1-x}Zr_xO_2$. It is apparent that the high-field polarization properties of the wurtzite ferroelectrics are characterized by high remanent polarizations coupled with high coercive fields. For example, most of the AlN-based compositions have remanent polarizations in excess of 100 $\mu C/cm^2$, with coercive fields that exceed 4 MV/cm at room temperature for measurements at 100 Hz.[13,14] It is apparent that Sc modifications lower the coercive field

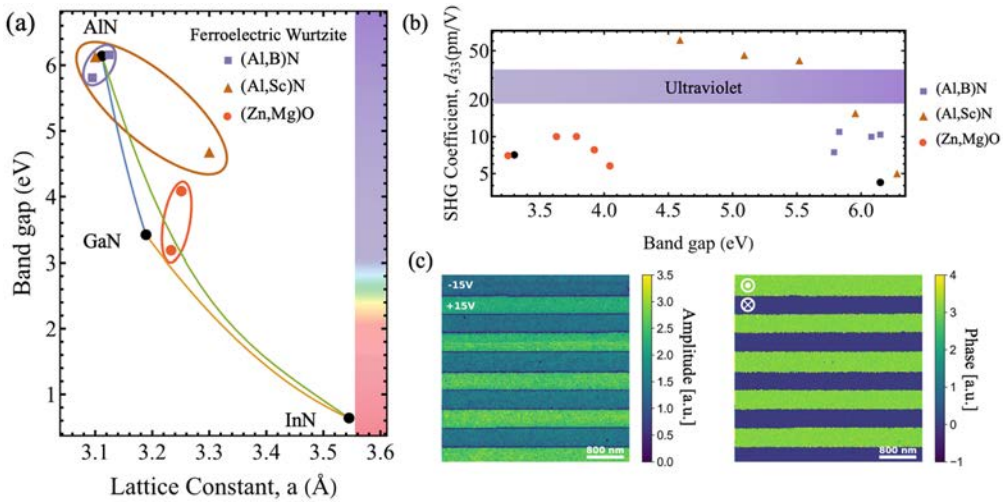

FIG. 5. (a) Experimental values for bandgap vs in-plane lattice constant of existing III-nitride semiconductors and new ternary wurtzite ferroelectrics of $Al_{1-x}B_xN$, $Al_{1-x}Sc_xN$, and $Zn_{1-x}Mg_xO$ alloys. The ellipses show trends for the alloy systems. (b) Measured second order nonlinear susceptibilities from SHG measurements for ternary wurtzite ferroelectrics. The purple bar highlights that all of these compounds show appreciable SHG behavior at ultraviolet wavelengths and enhanced SHG coefficients relative to binary constituents ZnO and AlN for most cation alloying contents. Periodic poling from DC bias in PFM measurements for 20 nm thick $Al_{1-x}B_xN$ ($x = 0.07$) films, generating uniform domains down to 400 nm in width, indicating suitably for quasi-phase matched heterostructures at ultraviolet wavelengths. Reproduced with permission from Suceava *et al.*, Opt. Mater. Express **13**, 1522 (2023). Copyright 2023 Optica Publishing Group under the terms of the Open Access Publishing Agreement.[97]

more than B, potentially due to a different polarization reversal pathway.

The coercive fields of $Zn_{1-x}Mg_xO$ wurtzites, like those of the AlN-based compositions, are strongly temperature dependent. As is typical of ferroelectric materials, in the wurtzites, there is not a single activation energy for polarization reversal. Instead, the temperature-dependent pseudo-activation energies are ~20 to 40 meV.[101] These are considerably below the activation energies that would be expected for an intrinsic coercive field (e.g., uniform switching of the polarization throughout the film volume at once) and strongly suggest the existence of mobile interfaces such as domain walls as the means of polarization reversal. In $Al_{1-x}B_xN$, the switching occurs through a non-polar intermediate structure, which is structurally reminiscent of an inversion domain wall in a nitride, or indeed a small slice of a feldspar-like structure. This allows the polarization reversal process, and the commensurate bond-breaking to be conducted a few atoms at a time, rather than simultaneously through the entire structure.

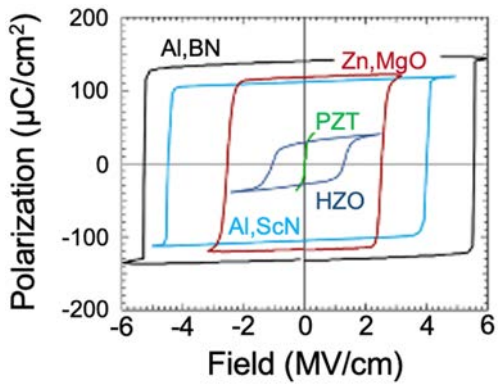

FIG. 6. Measured polarization-electric field hysteresis loops for ternary wurtzite ferroelectric materials and technologically relevant ferroelectrics HZO and PZT. It is noted that the coercive field is frequency dependent and the shape of the loops can be influenced by conduction mechanisms at high field, which are dependent on film thickness and measurement frequency.

In their as-deposited state, wurtzite ferroelectrics behave like linear dielectrics for the first several cycles and must be "woken-up" to display polarization switching. This has been shown in $Al_{1-x}B_xN$ and $Zn_{1-x}Mg_xO$, where the wake up process is highly rate dependent. If field cycles are a few Hz, full wake up will occur in one cycle, whereas 1 kHz cycling may require several hundred. In at least some cases, the wake-up phenomenon is related to the fact that films are unipolar (or nearly so) as grown and the process involves generating enough nuclei of the opposite orientation to enable full switching of the polarization. It is also noted that some ferroelectrics wurtzites have imprint and hence some voltage asymmetry in the measured P-E loops, which decreases after field cycling, which is linked to the wakeup process. Once woken up, the hysteresis loops of the wurtzite ferroelectrics are typically quite square, suggesting comparatively abrupt switching relative to many other ferroelectric materials. Recent work suggests that the nucleation rate goes through a maximum during the growth and impingement phases.[102] This differs from reports on switching in perovskite ferroelectrics, including the Kolmogorov–Avrami–Ishibashi (KAI) model,[103] or the nucleation limited switching (NLS) model.[104] The ultimate switching speeds of the wurtzite ferroelectrics are as-yet unknown.

It should be noted that there are numerous reports of hysteresis loops in the wurtzites that are rounded at the top and/or the bottom of the loop, indicating a substantial contribution of leakage currents. Artifacts of this type inflate the apparent remanent polarization. In

cases where sufficient power is available in the measurement electronics, this can be mitigated by measurements at higher frequencies. Where that is not possible, PUND measurements can be useful, though as usual, care should be taken when a small number is derived as the difference between two large numbers (that is, PUND measurements are useful but not fail-safe in very leaky samples).

In part because of the very high coercive fields characteristic of the wurtzite ferroelectrics to date, their data retention properties are excellent, considerably out-performing the polarization retention times of ferroelectrics such as PZT or $Hf_{1-x}Zr_xO_2$ (Fig. 7). For example, $Al_{0.93}B_{0.07}N$ films with W top and bottom electrodes retained >200 $\mu C/cm^2$ of opposite state signal margin after baking for 1000 h at 200 °C. In $Zn_{0.64}Mg_{0.36}O$, no polarization loss was observed over the same time frame. In $Al_{0.7}Sc_{0.3}N$, data can be retained for at least 1000 s exposures to 400 °C.[105] Even further, $Al_{1-x}Sc_xN$ retains its polarization state after heating to 1100 °C, demonstrating wurtzite ferroelectrics are the only ferroelectrics currently capable of operating in this extreme temperature regime.[50] This is reasonable, since it is likely that none of wurtzite ferroelectrics demonstrated to date undergo a Curie temperature to a non-ferroelectric prototype phase prior to melting. Thus, the change of spontaneous polarization with temperature is not accelerated as the vicinity of a phase transition is not reached.

Among the remaining challenges in the wurtzite ferroelectrics is demonstration of high cycle lifetime on bipolar switching. Many of the available films undergo dielectric breakdown following cycling of thousands to millions of cycles. These aspects will have to be improved to enable integrated memory applications where cycling requirements necessitate at least 10^{15} cycles. It is anticipated that this cycling would be improved as deleterious film defect densities decrease (especially at electrode interfaces as film thickness decreases) to allow for continued voltage scaling. Overall, cycling performance is expected to increase the most if the coercive fields of the wurtzites could be reduced without significantly degrading the bandgap.

VII. FIRST PRINCIPLES CALCULATIONS

To further aid in the discovery of novel highly piezoelectric and ferroelectric wurtzite materials and improve their suitability for memory applications, computational methods such as the density functional theory (DFT), molecular dynamics, and machine learning (ML) have been employed to uncover the structure–property relationships, especially those that govern the switching mechanisms in alloyed wurtzite semiconductors. Although significant theoretical work has gone into understanding the physical properties of wurtzite semiconductors such as AlN and GaN, ferroelectric behavior opens up new opportunities to understand the physics of wurtzite materials. Previously, the absolute magnitudes of spontaneous polarization in wurtzite semiconductors could not be experimentally measured as the spontaneous polarizations could not be reversed. Heterojunctions, such as $A_{1-x}Ga_xN$-GaN, offered the possibility to measure polarization discontinuities and relative polarization values, but ferroelectric behavior changed this notion. Thus, a fundamental understanding of polarization in wurtzites pays dividends to heterostructures that do not even utilize the polarization reversal (e.g., commercial $Al_{1-x}Ga_xN$-GaN transistors as power amplifiers).

To this end, several additional important ongoing areas for wurtzite ferroelectrics involve the understanding and engineering of coercive field values, ferroelectric domain nucleation and growth, and interfacial effects with substrates. For example, one of the drawbacks to technological adoption of wurtzite materials for integrated memory applications is the ultra-large coercive field. The large coercive fields (>2 MV/cm) exceed what is needed to ensure a sufficient memory window and threshold voltage stability in scaled devices. Strategies to lower the coercive field involve insight from first principles calculations and work toward understanding how the structure transitions from metal polarity to nitrogen polarity or vice versa.[12,106] A primary way to elucidate the polarization reversal mechanism from DFT is to calculate the minimum energy pathway between the different bulk polarization states using the nudged elastic band (NEB) method.[107] Recently, NEB simulations predicted a lower reversal barrier in $Al_{1-x}B_xN$ compared to AlN.[59] Moreover, the intermediate state in $Al_{1-x}B_xN$ is an anti-polar state rather than the hexagonal-BN phase in AlN. This type of analysis provides structural insight into the effects of alloying elements on the bulk wurtzite that enable ferroelectricity, enabling control over the coercive field. As an extension of DFT, high-throughput methods have been used to discover and characterize new wurtzite solid solutions. Using these larger datasets of possible materials, machine learning (ML) featurization has been employed to understand the structure–property relationships that govern these ferroelectric responses and discover dopants to improve the material response. An example of this is shown in Fig. 8.

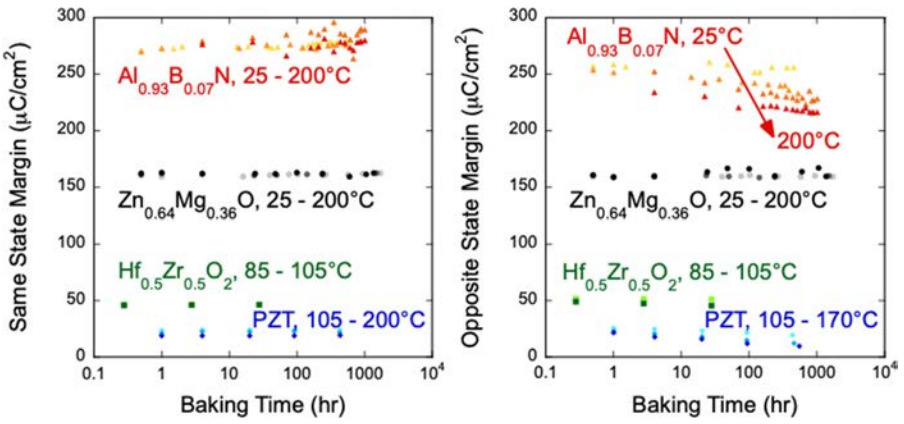

FIG. 7. Polarization retention as a function of bake temperature and time for wurtzite ferroelectrics compared to commercial PZT and $Hf_{0.5}Zr_{0.5}O_2$ films. Wurtzite $Al_{0.93}B_{0.07}N$ and $Zn_{0.64}Mg_{0.36}O$ show excellent same state polarization margin.

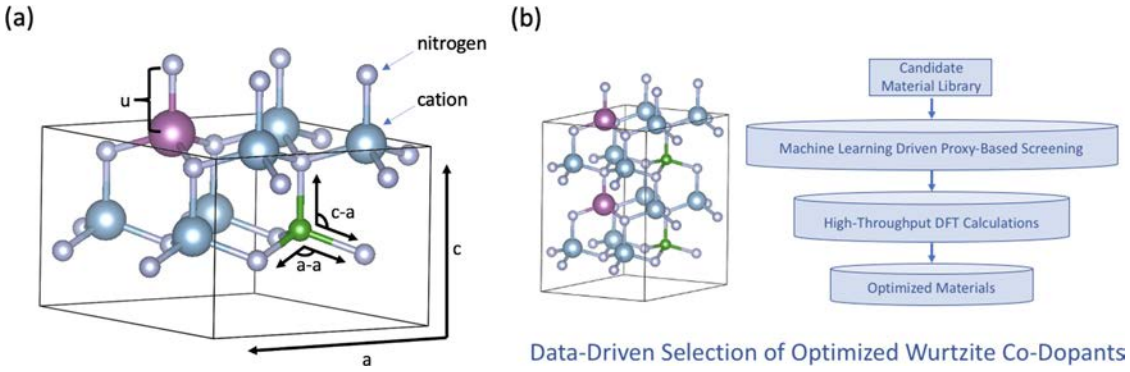

FIG. 8. (a) Schematic of wurtzite supercell in VESTA software utilized in simulations, utilizing different cations and analyzing the changes in internal bond angles (a–a, c–a) and internal parameter (u). *c* and *a* correspond to the crystallographic axes. The atoms shown depict atomic radii (e.g., Al and N), not ionic radii (Al^{+3} and N^{-3}). Magnitudes of spontaneous and piezoelectric polarization in the wurtzites are known to be sensitive to *c*/*a* ratios, u values, and bond angles. (b) Process flow utilizing machine learning and first principles calculations to accelerate materials discovery and design.

Another promising avenue to enhance device functionality for wurtzite ferroelectrics is lowering the coercive field and thus leakage current densities using strain, both local and interfacial. Previous work has shown that the lattice parameters, local bond distances, and degree of bond ionicity in wurtzites are strong indicators of overall responsiveness to an applied electric field.[44,108–111] Moreover, first-principles studies have demonstrated that applying an in-plane *a*-*b* expansion (e.g., tensile strain) during thin film growth is expected to lower the barrier of polarization reversal.[112] Using DFT and ML in the future is expected to pay dividends toward determining the impacts of defects, doping, and interfaces on the material strain, which vary based on deposition technique. Combined, these are crucial action levers to control the ferroelectric properties of wurtzite-based materials.

VIII. DEVICES AND EMERGING APPLICATIONS

The emerging ecosystem of ferroelectric wurtzite materials requires careful heterostructure design to efficiently emphasize the new features these materials offer and minimize deleterious effects that accompany these new properties. For example, the large polarizations in ferroelectric wurtzites necessitate electrodes with large carrier concentrations to compensate the polarization charge. This is prevalent when utilizing degenerately doped semiconductors as electrodes or incorporation in heterostructures with 2DEGs and 2DHGs in HEMT heterostructures. Incorporating ferroelectric behavior into nitride HEMTs holds the promise of integrating memory functionality with digital electronics. Recent reports of ferroelectric nitride HEMT heterostructures have demonstrated sub-60 mV/decade subthreshold slopes at room temperature[113,114] and gain at frequencies in excess of 100 GHz.[115] Future work in this area will involve exploring the aspects of ultra-thin ferroelectric nitride layers and heterostructure design and depolarization effects. In addition, the prospect of negative drain induced barrier lowering (nDIBL) associated with ferroelectric behavior would be beneficial to improving the limitations set by short channel effects in scaled devices.[116,117] The large electric fields (e.g., >3 MV/cm) associated with polarization reversal in ferroelectric wurtzites imply challenges when integrating with GaN devices (the GaN breakdown field is ∼3 to 3.4 MV/cm, depending on doping levels)[118,119] and necessitate use of electrode geometries and heterostructures that minimize electric field crowding to prevent premature dielectric breakdown and device failure. Field plate devices and associated heterostructures that reduce peak electric fields are expected to improve high-field performance and stability. In addition, polarization-graded heterostructures,[120–122] made possible by the polarization-induced doping, provide opportunities to reduce peak electric fields and assess the physics of ferroelectric three-dimensional electron gases (3DEGs) and generate built-in p-n junctions from polarization fields. Also, the strong non-linear optical responses shown by wurtzite ferroelectrics come at the expense of increased optical losses at visible wavelengths and beyond. These losses need to be reduced to allow for light propagation on centimeter length scales and to take advantage of the quasi-phase matching offered from periodic poling of domain arrays. The ability to precisely etch and pattern heterostructures, generate materials with low defect densities, as well as smooth domain wall interfaces, will be beneficial for reducing optical losses in waveguides and in devices incorporating nonlinear phenomena. For acoustic devices, periodically poled resonators utilizing $Al_{1-x}Sc_xN$ alloys have recently shown promise in generating higher frequency harmonic modes.[123,124] Improving the quality factor at higher frequencies through heterostructure design and/or materials development will continue to be a significant challenge as scaling to high frequencies comes with associated tradeoffs.

The aspects in the previous paragraph also apply to existing device designs studied for CMOS integrated memory. For example, three common ferroelectric memory devices being studied with $Hf_{1-x}Zr_xO_2$ alloys are ferroelectric FETs (FeFETs), ferroelectric tunnel junctions (FTJs), and ferroelectric random access memories (FeRAM) in the form of 1 transistor-1 capacitor (1T-1C) architectures.[125] For wurtzite-based FeFETs, the large remanent polarization values cannot be completely compensated by conventional semiconductor channels. For reference, 100 $\mu C/cm^2$ would equate to a $6.25 \times 10^{14}/cm^2$ mobile carrier sheet charge density. An additional approach could be to integrate wurtzites with amorphous In_2O_3, which has a large carrier n type concentration of $\sim 1 \times 10^{20}/cm^3$ while still maintaining a large electron saturation velocity of $\sim 1 \times 10^7$ cm/s.[126,127] Tuning the In_2O_3 thickness will tailor the total charge that can be accumulated at the interface and allow for threshold voltage modulation. For FTJs and FeRAM, the large remanent polarizations of wurtzites are expected to

be advantageous to providing more tunneling current modulation and more charge from the capacitor, respectively. Recent work demonstrating ternary content-addressable memory (TCAM) based on back-end-of line (BEOL) compatible $Al_{1-x}Sc_xN$ ferroelectric diodes is compelling.[128] FeRAM with wurtzites is feasible with large polarization charges available, allowing capacitor area scaling reduction for the same charge sense amplifier typically used in FeRAM. Both sets of devices would require extensive work in reduction in the films' coercive fields to operate at CMOS technology voltages (~3.3 to 0.7 V) and demonstrate low leakage currents for the FeRAM. Opportunities exist for ferroelectrics in NAND type architectures, which operate at larger voltages (~15 to 20 V) and at slower speeds and fewer endurance cycles than the main memory cache. CMOS compatible ferroelectrics offer the ability to lower the NAND programming voltage[129] and reduce the number of layers in the stack, thus improving threshold voltage shift variation concerns and improving memory density. However, the ability to aggressively stack ferroelectric capacitors in 3D geometries to compete with NAND density remains an open area of investigation and innovation.

IX. CONCLUSIONS

Ferroelectric wurtzite materials are being extensively studied for potential use in integrated memory. In addition, ferroelectric wurtzites offer the ability to merge logic and memory functionalities in digital electronics and demonstrate enhanced non-linear optical responses for on-chip systems and integration in existing III-nitride photonic platforms. Significant progress has been made in recent years in demonstrating ferroelectricity in ultrathin layers toward CMOS voltage ranges, which also opens up applications in quantum heterostructures and allows for increased flexibility in heterostructure processing and design, such as strain engineering. Future research directions can build on the knowledge gained from $Hf_{1-x}Zr_xO_2$ and related systems to further drive voltage reductions and improve fatigue and endurance performance. In addition to competing with $Hf_{1-x}Zr_xO_2$ for use in integrated memory, ferroelectric wurtzites hold distinct advantages for use in high voltage, high temperature, and harsh environment memory applications due to the strong chemical bonds in the wurtzite crystal structure. A more thorough understanding of defect densities that contribute to leakage currents, polarization reversal mechanisms toward lowering the coercive field, and synthesis and design of new materials with reduced defects and different defect tolerances will help guide further heterostructure design and the ultimate utilization of this emerging class of materials.

ACKNOWLEDGMENTS

The authors would like to acknowledge support from the defense advanced research projects agency (DARPA) tunable ferroelectric nitrides (TUFEN) program under the supervision of Dr. Ronald Polcawich and Dr. Ali Keshavarzi (Grant Nos. W911NF-20-2-0274 and HR0011-20-9-0047). The data presented in Figs. 1, 2(c), 2(e), 3, 4, 5, 6, 7, and 8 are based upon work supported by the U.S. Department of Energy, Office of Science, Office of Basic Energy Sciences Energy Frontier Research Centers program under Award No. DE-SC0021118. Sandia National Laboratories is a multimission laboratory managed and operated by National Technology and Engineering Solutions of Sandia, LLC, a wholly owned subsidiary of Honeywell International Inc., for the U.S. Department of Energy's National Nuclear Security Administration under Contract No. DE-NA0003525. This paper describes objective technical results and analysis. Any subjective views or opinions that might be expressed in the paper do not necessarily represent the views of the U.S. Department of Energy or the United States Government.

AUTHOR DECLARATIONS

Conflict of Interest

The authors have no conflicts to disclose.

Author Contributions

Joseph Casamento: Conceptualization (lead); Data curation (equal); Resources (equal); Writing – original draft (lead); Writing – review & editing (equal). **Steven Baksa:** Data curation (equal); Resources (equal); Software (equal); Writing – review & editing (equal). **Drew Behrendt:** Data curation (equal); Resources (equal); Software (equal); Writing – review & editing (equal). **Sebastian Calderon:** Data curation (equal); Resources (equal); Writing – review & editing (equal). **Devin Goodling:** Data curation (supporting); Resources (equal); Writing – review & editing (equal). **John Hayden:** Data curation (equal); Resources (equal); Writing – review & editing (equal). **Fan He:** Data curation (equal); Resources (equal); Writing – review & editing (equal). **Leonard Jacques:** Data curation (equal); Resources (equal); Writing – review & editing (equal). **Seung Hoon Lee:** Data curation (supporting); Writing – review & editing (equal). **Walter J. Smith:** Data curation (equal); Resources (equal); Writing – review & editing (equal). **Albert Suceava:** Data curation (equal); Resources (equal); Writing – review & editing (equal). **Quyen Tran:** Data curation (supporting); Resources (equal); Writing – review & editing (equal). **Xiaojun Zheng:** Data curation (supporting); Resources (equal); Writing – review & editing (equal). **Rui Zu:** Data curation (equal); Resources (equal); Writing – review & editing (equal). **Thomas Beechem:** Data curation (equal); Resources (equal); Writing – review & editing (equal). **Ismaila Dabo:** Data curation (equal); Resources (equal); Software (equal); Writing – review & editing (equal). **Elizabeth C. Dickey:** Data curation (equal); Resources (equal); Writing – review & editing (equal). **Giovanni Esteves:** Data curation (supporting); Resources (equal); Writing – review & editing (equal). **Venkatraman Gopalan:** Data curation (equal); Software (equal); Writing – review & editing (equal). **Michael David Henry:** Data curation (supporting); Software (supporting); Writing – review & editing (equal). **Jon F. Ihlefeld:** Data curation (equal); Resources (equal); Writing – review & editing (equal). **Thomas N. Jackson:** Data curation (supporting); Resources (equal); Writing – review & editing (equal). **Sergei V. Kalinin:** Data curation (supporting); Resources (supporting); Writing – review & editing (equal). **Kyle Patrick Kelley:** Data curation (equal); Resources (equal); Writing – review & editing (equal). **Yongtao Liu:** Data curation (equal); Resources (equal); Writing – review & editing (equal). **Andrew M. Rappe:** Data curation (equal); Software (equal); Writing – review & editing (equal). **Joan M. Redwing:** Data curation (supporting); Resources (supporting); Writing – review & editing (equal). **Susan Trolier-McKinstry:** Data curation (equal); Funding acquisition (lead); Resources (equal); Writing – review & editing (equal). **Jon-Paul Maria:** Data curation (equal); Funding acquisition (lead); Resources (equal); Writing – review & editing (equal).

DATA AVAILABILITY

The data that support the findings of this study are available from the corresponding author upon reasonable request.

REFERENCES

[1]M.-A. Dubois, P. Muralt, and V. Plessky, in *IEEE International Ultrasonics Symposium* (IEEE, Caesars Tahoe, NV, 1999), pp. 907–910.
[2]M. D. Hodge, R. Vetury, S. R. Gibb, M. Winters, P. Patel, M. A. McLain, Y. Shen, D. H. Kim, J. Jech, K. Fallon, R. Houlden, D. M. Aichele, and J. B. Shealy, in *IEEE International Electron Devices Meeting (IEDM)* (IEEE, San Francisco, CA, 2017), pp. 25.6.1–25.6.4.
[3]A. Hickman, R. Chaudhuri, S. J. Bader, K. Nomoto, K. Lee, H. G. Xing, and D. Jena, IEEE Electron Device Lett. **40**, 1293 (2019).
[4]S. M. Islam, K. Lee, J. Verma, V. Protasenko, S. Rouvimov, S. Bharadwaj, H. (Grace) Xing, and D. Jena, Appl. Phys. Lett. **110**, 041108 (2017).
[5]Z. Zhang, M. Kushimoto, T. Sakai, N. Sugiyama, L. J. Schowalter, C. Sasaoka, and H. Amano, Appl. Phys. Express **12**, 124003 (2019).
[6]H. Then, M. Radosavljevic, P. Koirala, N. Thomas, N. Nair, I. Ban, T. Talukdar, P. Nordeen, S. Ghosh, S. Bader, T. Hoff, T. Michaelos, R. Nahm, M. Beumer, N. Desai, P. Wallace, V. Hadagali, H. Vora, A. Oni, X. Weng, K. Joshi, I. Meric, C. Nieva, S. Rami, and P. Fischer, in *Proceedings of the IEEE International Electron Devices Meeting (IEDM)* (IEEE, San Francisco, CA, 2021), pp. 11.1.1–11.1.4.
[7]H. W. Then, M. Radosavljevic, Q. Yu, A. Latorre-Rey, H. Vora, S. Bader, I. Momson, D. Thomson, M. Beumer, P. Koirala, J. Peck, A. Oni, T. Hoff, R. Jordan, T. Michaelos, N. Nair, P. Nordeen, A. Vyatskikh, I. Ban, A. Zubair, S. Rami, and P. Fischer, IEEE Microwave Wireless Technol. Lett. **33**, 835 (2023).
[8]O. Ambacher, J. Smart, J. R. Shealy, N. G. Weimann, K. Chu, M. Murphy, W. J. Schaff, L. F. Eastman, R. Dimitrov, L. Wittmer, M. Stutzmann, W. Rieger, and J. Hilsenbeck, J. Appl. Phys. **85**, 3222 (1999).
[9]O. Ambacher, B. Foutz, J. Smart, J. R. Shealy, N. G. Weimann, K. Chu, M. Murphy, A. J. Sierakowski, W. J. Schaff, L. F. Eastman, R. Dimitrov, A. Mitchel, and M. Stutzmann, J. Appl. Phys. **87**, 334 (2000).
[10]C. Wood and D. Jena, *Polarization Effects in Semiconductors -From Ab Initio Theory to Device Applications* (Springer, 2008).
[11]R. Chaudhuri, S. J. Bader, Z. Chen, D. A. Muller, H. G. Xing, and D. Jena, Science **365**, 1454 (2019).
[12]M. Akiyama, T. Kamohara, K. Kano, A. Teshigahara, Y. Takeuchi, and N. Kawahara, Adv. Mater. **21**, 593 (2009).
[13]S. Fichtner, N. Wolff, F. Lofink, L. Kienle, and B. Wagner, J. Appl. Phys. **125**, 114103 (2019).
[14]A. Konishi, T. Ogawa, C. A. J. Fisher, A. Kuwabara, T. Shimizu, S. Yasui, M. Itoh, and H. Moriwake, Appl. Phys. Lett. **109**, 102903 (2016).
[15]J. Hayden, M. D. Hossain, Y. Xiong, K. Ferri, W. Zhu, M. V. Imperatore, N. Giebink, S. Trolier-McKinstry, I. Dabo, and J. P. Maria, Phys. Rev. Mater. **5**, 044412 (2021).
[16]K. Ferri, S. Bachu, W. Zhu, M. Imperatore, J. Hayden, N. Alem, N. Giebink, S. Trolier-McKinstry, and J. P. Maria, J. Appl. Phys. **130**, 044101 (2021).
[17]M. Akiyama, K. Kano, and A. Teshigahara, Appl. Phys. Lett. **95**, 162107 (2009).
[18]N. Kurz, A. Ding, D. F. Urban, Y. Lu, L. Kirste, N. M. Feil, A. Zukauskaite, and O. Ambacher, J. Appl. Phys. **126**, 075106 (2019).
[19]J. Casamento, H. Lee, T. Maeda, V. Gund, K. Nomoto, L. van Deurzen, W. Turner, P. Fay, S. Mu, C. G. Van de Walle, A. Lal, H. G. Xing, and D. Jena, Appl. Phys. Lett. **120**, 152901 (2022).
[20]J. Casamento, C. S. Chang, Y.-T. Shao, J. Wright, D. A. Muller, H. G. Xing, and D. Jena, Appl. Phys. Lett. **117**, 112101 (2020).
[21]V. Yoshioka, J. Lu, Z. Tang, J. Jin, R. H. Olsson III, and B. Zhen, APL Mater. **9**, 101104 (2021).
[22]Y. Song, C. Perez, G. Esteves, J. S. Lundh, C. B. Saltonstall, T. E. Beechem, J. I. Yang, K. Ferri, J. E. Brown, Z. Tang, J. P. Maria, D. W. Snyder, R. H. Olsson III, B. A. Griffin, S. E. Trolier-McKinstry, B. M. Foley, and S. Choi, ACS Appl. Mater. Interfaces **13**, 19031 (2021).
[23]P. Wang, D. Wang, S. Mondal, M. Hu, J. Liu, and Z. Mi, Semicond. Sci. Technol. **38**, 043002 (2023).
[24]K. H. Kim, I. Karpov, R. H. Olsson III, and D. Jariwala, Nat. Nanotechnol. **18**, 422 (2023).
[25]L. Xia, Z. Liu, and Z. Taskinen, J. Alloys Compd. **687**, 827 (2016).
[26]P. Wang, D. Wang, N. M. Vu, T. Chiang, J. T. Heron, and Z. Mi, Appl. Phys. Lett. **118**, 223504 (2021).
[27]P. Wang, D. Wang, S. Mondal, and Z. Mi, Appl. Phys. Lett. **121**, 023501 (2022).
[28]D. Wang, S. Mondal, J. Liu, M. Hu, P. Wang, S. Yang, D. Wang, Y. Xiao, Y. Wu, T. Ma, and Z. Mi, Appl. Phys. Lett. **123**, 033504 (2023).
[29]M. Bosund, T. Sajavaara, M. Laitinen, T. Huhtio, M. Putkonen, V.-M. Airaksinen, and H. Lipsanen, Appl. Surf. Sci. **257**(17), 7827 (2011).
[30]M. Alevli, C. Ozgit, I. Donmez, and N. Biyikli, Phys. Status Solidi A **209**, 266 (2012).
[31]N. Nepal, S. B. Qadri, J. K. Hite, N. A. Mahadik, M. A. Mastro, and C. R. Eddy, Appl. Phys. Lett. **103**, 082110 (2013).
[32]N. A. Strnad, W. L. Sarney, G. B. Rayner, R. R. Benoit, G. R. Fox, R. Q. Rudy, T. J. Larrabee, J. Shallenberger, and J. S. Pulskamp, J. Vac. Sci. Technol., A **40**, 042403 (2022).
[33]S. Leone, J. Ligl, C. Manz, L. Kirste, T. Fuchs, H. Menner, M. Prescher, J. Wiegert, A. Žukauskaitė, R. Quay, and O. Ambacher, Phys. Status Solidi RRL **14**, 1900535 (2020).
[34]C. Manz, S. Leone, L. Kirste, J. Ligl, K. Frei, T. Fuchs, M. Prescher, P. Waltereit, M. A. Verheijen, and A. Graff, Semicond. Sci. Technol. **36**, 034003 (2021).
[35]I. Streicher, S. Leone, L. Kirste, C. Manz, P. Straňák, M. Prescher, P. Waltereit, M. Mikulla, R. Quay, and O. Ambacher, Phys. Status Solidi RRL **17**, 2200387 (2022).
[36]S. Leone, I. Streicher, M. Prescher, P. Straňák, and L. Kirste, Phys. Status Solidi RRL **17**, 2300091 (2023).
[37]K. Uesugi and H. Miyake, Jpn. J. Appl. Phys., Part 1 **60**, 120502 (2021).
[38]S. A. Anggraini, M. Uehara, K. Hirata, H. Yamada, and M. Akiyama, Sci. Rep. **10**, 4369 (2020).
[39]N. Stolyarchuk, T. Markurt, A. Courville, K. March, J. Zuniga-Perez, P. Vennegues, and M. Albrecht, Sci. Rep. **8**, 14111 (2018).
[40]S. Mohn, N. Stolyarchuk, T. Markurt, R. Kirste, M. P. Hoffman, R. Collazo, A. Courville, R. Di Felice, Z. Sitar, P. Vennegues, and M. Albrecht, Phys. Rev. Appl. **5**, 054004 (2016).
[41]L. A. Bendersky, I. Takeuchi, K. S. Chang, W. Yang, S. Hullavarad, and R. D. Vispute, J. Appl. Phys. **98**, 083526 (2005).
[42]C. Höglund, J. Birch, B. Alling, J. Bareno, Z. Czignary, P. O. A. Persson, G. Wingqvist, A. Zukauskaite, and L. Hultman, J. Appl. Phys. **107**, 123515 (2010).
[43]J. Su, S. Fichtner, M. Z. Ghori, N. Wolff, Md. R. Islam, A. Lotnyk, D. Kaden, F. Niekel, L. Kienle, B. Wagner, and F. Lofink, Micromachines **13**, 783 (2022).
[44]K. Yazawa, J. S. Mangum, P. Gorai, G. L. Brennecka, and A. Zakutayev, J. Mater. Chem. C **10**, 17557 (2022).
[45]C. Liu, Q. Wang, W. Yang, T. Cao, L. Chen, M. Li, F. Liu, D. K. Loke, J. Kang, and Y. Zhu, in *Proceedings of IEEE International Electron Devices Meeting (IEDM)* (IEEE, San Francisco, CA, 2022), pp. 8.1.1–8.1.4.
[46]G. Schönweger, Md. R. Islam, N. Wolff, A. Petraru, L. Kienle, H. Kohlstedt, and S. Fichtner., Phys. Status Solidi RRL **17**, 2200312 (2023).
[47]C. Liu, M. Li, B. Chen, Y. Zhang, Y. Zhu, and N. Wang, J. Micromech. Microeng. **32**, 034002 (2022).
[48]D. Wang, J. Zhang, Z. Tang, M. D'Agati, P. S. M. Gharavi, X. Liu, D. Jariwala, E. A. Stach, and R. H. Olsson III, in *Proceedings of Joint Conference of the IEEE International Frequency Control Symposium and International Symposium on Applications of Ferroelectrics (IFCS-ISAF)* (IEEE, Keystone, CO, 2020), pp. 1–4.
[49]X. Zhang, E. A. Stach, J. W. Meng, and C. A. Meng, Nanoscale Horiz. **8**, 674 (2023).
[50]M. R. Islam, N. Wolff, M. Yassine, G. Schonweger, B. Christian, H. Kohlstedt, O. Ambacher, F. Lofink, L. Kienle, and S. Fichtner, Appl. Phys. Lett. **118**, 232905 (2021).
[51]R. Guido, P. D. Lomenzo, M. Islam, N. Wolff, M. Gremmel, G. Schonweger, H. Kohlstedt, L. Kienle, T. Mikolajick, S. Fichtner, and U. Schroeder, ACS Appl. Mater. Interfaces **15**, 7030 (2023).
[52]D. Drury, K. Yazawa, A. Mis, K. Talley, A. Zakutayev, and GL. Brennecka, Phys. Status Solidi RRL **15**, 2100043 (2021).

[53]G. Schönweger, A. Petraru, Md. R. Islam, N. Wolff, B. Haas, A. Hammud, C. Koch, L. Kienle, H. Kohlstedt, and S. Fichtner, Adv. Funct. Mater. **32**, 2109632 (2022).
[54]P. Wang, D. Wang, Y. Bi, B. Wang, J. Schwartz, R. Hovden, and Z. Mi, Appl. Phys. Lett. **120**, 012104 (2022).
[55]C. S. Sandu, F. Parsapour, S. Mertin, V. Pashchenko, R. Matloub, T. LaGrange, B. Heinz, and P. Muralt, Phys. Status Solidi A **216**, 1800569 (2019).
[56]S. Calderon, S. D. Funni, and E. C. Dickey, Microsc. Microanal. **28**, 2047 (2022).
[57]R. D. King-Smith and D. Vanderbilt, Phys. Rev. B **47**, 1651 (1993).
[58]D. Vanderbilt and R. D. King-Smith, Phys. Rev. B **48**, 4442 (1993).
[59]S. Calderon, J. Hayden, S. M. Baksa, W. Tzou, S. Trolier-McKinstry, I. Dabo, J. P. Maria, and E. C. Dickey, Science **380**, 1034 (2023).
[60]W. Zhu, J. Hayden, F. He, J. I. Yang, P. Tipsawat, M. D. Hossain, J. P. Maria, and S. Trolier-McKinstry, Appl. Phys. Lett. **119**, 062901 (2021).
[61]C. E. Dreyer, A. Janotti, C. G. Van de Walle, and D. Vanderbilt, Phys. Rev. X **6**, 021038 (2016).
[62]N. Wolff, S. Fichtner, B. Haas, M. Islam, F. Niekiel, M. Kessel, O. Ambacher, C. Koch, B. Wagner, F. Lofink, and L. Kienle, J. Appl. Phys. **129**, 034103 (2021).
[63]S. E. Zeltmann, S. L. Hsu, H. G. Brown, S. Susarla, A. Minor, and C. Ophus, Microsc. Microanal. **29**, 256 (2023).
[64]H. Zhang, J. Persson, A. Papamichail, T. Chen, Jr., P. O. A. Persson, P. P. Paskov, and V. Darakchieva, J. Appl. Phys. **131**, 055701 (2022).
[65]M. Park, J. J. Cuomo, B. J. Rodriguez, W.-C. Yang, R. J. Nemanich, and O. Ambacher, J. Appl. Phys. **93**, 9542 (2003).
[66]R. Kirste, S. Mita, M. P. Hoffman, L. Hussey, W. Guo, I. Bryan, Z. Bryan, J. Tweedle, M. Gerhold, A. Hoffman, R. Collazo, and Z. Sitar, Phys. Status Solidi C **11**, 261 (2014).
[67]R. Kirste, R. Collazo, G. Callsen, M. R. Wagner, T. Kure, J. S. Reparaz, S. Mita, J. Xie, A. Rice, J. Tweedle, Z. Sitar, and A. Hoffman, J. Appl. Phys. **110**, 093503 (2011).
[68]G. Schönweger, N. Wolff, Md. R. Islam, M. Gremmel, A. Petraru, L. Kienle, H. Kohlstedt, and S. Fichtner, Adv. Sci. **10**, 2302296 (2023).
[69]L. Li, L. Xie, and X. Pan, Rep. Prog. Phys. **82**, 126502 (2019).
[70]Z. Liu, X. Wang, X. Ma, Y. Yang, and D. Wu, Appl. Phys. Lett. **122**, 122901 (2023).
[71]A. K. Tagantsev, L. E. Cross, and J. Fousek, *Domains in Ferroic Crystals and Thin Films* (Springer, 2010).
[72]A. L. Gruverman, J. Hatano, and H. Tokumoto, Jpn. J. Appl. Phys., Part 1 **36**, 2207 (1997).
[73]K. Franke, J. Besold, W. Haessler, and C. Seegebarth, Surf. Sci. **302**, L283 (1994).
[74]S. Jesse, H. N. Lee, and S. V. Kalinin, Rev. Sci. Instrum. **77**, 073702 (2006).
[75]B. J. Rodriguez, A. Gruverman, A. I. Kingon, and R. J. Nemanich, J. Cryst. Growth **246**, 252 (2002).
[76]W. Zhu, F. He, J. Hayden, Z. Fan, J. I. Yang, J. P. Maria, and S. Trolier-McKinstry, Adv. Electron. Mater. **8**, 2100931 (2022).
[77]C. W. Bark, P. Sharma, Y. Wang, S. H. Baek, S. Lee, S. Ryu, C. M. Folkman, T. R. Paudel, A. Kumar, S. V. Kalinin, A. Sokolov, E. Y. Tsymbal, M. S. Rzchowski, A. Gruverman, and C. B. Eom, Nano Lett. **12**, 1765 (2012).
[78]A. Kumar, T. M. Arruda, Y. Kim, I. N. Ivanov, S. Jesse, C. W. Bark, N. C. Bristowe, E. Artacho, P. B. Littlewood, C. B. Eom, and S. V. Kalinin, ACS Nano **6**, 3841 (2012).
[79]Z. Liu, Y. Guo, J. Yan, Y. Zeng, J. Wang, and J. Li, Appl. Phys. Express **14**, 085501 (2021).
[80]A. D. Westwood, R. A. Youngman, M. R. McCartney, A. N. Cormack, and M. R. Notis, J. Mater. Res. **10**, 1270 (1995).
[81]T. Koppe, H. Hofsäss, and U. Vetter, J. Lumin. **178**, 267 (2016).
[82]Q. Zhou, Z. Zhang, H. Li, S. Golovynskyi, X. Tang, H. Wu, J. Wang, and B. Li, APL Mater. **8**, 081107 (2020).
[83]S.-L. Tsai, T. Hoshii, H. Wakabayashi, K. Tsutsui, T. K. Chung, E. Y. Chang, and K. Kakushima, Jpn. J. Appl. Phys., Part 1 **61**, SJ1005 (2022).
[84]J. Kataoka, S.-L. Tsai, T. Hoshii, H. Wakabayashi, K. Tsutsui, and K. Kakushima, Jpn. J. Appl. Phys., Part 1 **60**, 030907 (2021).
[85]L. Peters, C. Margenfeld, J. Krugener, C. Ronning, and A. Waag, Phys. Status Solidi A **220**, 2200485 (2023).
[86]S. Nakamura, T. Mukai, M. Senoh, and N. Iwasa, Jpn. J. Appl. Phys., Part 2 **31**, L139 (1992).
[87]S. Nakamura, N. Iwasa, M. Senoh, and T. Mukai, Jpn. J. Appl. Phys., Part 1 **31**, 1258 (1992).
[88]S. Nakamura, Adv. Mater. **8**, 689 (1996).
[89]S. Nakamura, Ann. Phys. **527**, 335 (2015).
[90]N. Vermeulen, D. Espinosa, A. Ball, J. Ballato, P. Boucaud, G. Boudebs, C. L. A. V. Campos, P. Dragic, A. S. L. Gomes, M. J. Huttunen, N. Kinsey, R. Mildren, D. Neshev, L. A. Padilha, M. Pu, R. Secondo, E. Tokunaga, D. Turchinovich, J. Yan, K. Yvind, K. Dolgaleva, and E. W. Van Stryland, J. Phys. Photonics **5**, 035001 (2023).
[91]A. P. Anthur, H. Zhang, Y. Yakimov, J. R. Ong, D. Kalashnikov, A. I. Kuznetsov, and L. Krivitsky, Opt. Express **29**, 10307 (2021).
[92]G. D. Boyd, R. C. Miller, K. Nassau, W. L. Bond, and A. Savage, Appl. Phys. Lett. **5**, 234 (1964).
[93]X. Liu, A. W. Bruch, and H. X. Tang, Adv. Opt. Photonics **15**, 236 (2023).
[94]Z. Tang, G. Esteves, and R. H. Olsson III, J. Appl. Phys. **134**, 114101 (2023).
[95]M. Alexe and U. Gosele, *Wafer Bonding—Applications and Technology* (Springer 2004).
[96]A. Bartasyte, S. Margueron, T. Baron, S. Oliveri, and P. Boulet, Adv. Mater. Interfaces **4**, 1600998 (2017).
[97]A. Suceava, J. Hayden, K. P. Kelley, Y. Xiong, B. Fazlioglu-Yalcin, I. Dabo, S. Trolier-McKinstry, J. P. Maria, and V. Gopalan, Opt. Mater. Express **13**, 1522 (2023).
[98]R. Zu, G. Ryu, K. P. Kelley, S. M. Baksa, L. C. Jacques, B. Wang, K. Ferri, J. He, L. Q. Chen, I. Dabo, S. Trolier-McKinstry, J. P. Maria, and V. Gopalan, Adv. Phys. Res. **2**, 2300003 (2023).
[99]X. Yuan, T. Yamada, and L. Meng, Appl. Phys. Lett. **121**, 152903 (2022).
[100]D. Wang, P. Wang, B. Wang, and Z. Mi, Appl. Phys. Lett. **119**, 111902 (2021).
[101]K. Coleman, S. Shetty, B. Hanrahan, W. Zhu, and S. Trolier-McKinstry, J. Appl. Phys. **128**, 114102 (2020).
[102]K. Yazawa, J. Hayden, J. P. Maria, W. Zhu, S. Trolier-McKinstry, A. Zakutayev, and G. L. Brennecka, Mater. Horiz. **10**, 2936 (2023).
[103]Y. Ishibashi and Y. Takagi, J. Phys. Soc. Jpn. **31**, 506 (1971).
[104]A. K. Tagantsev, I. Stolichnov, N. Setter, J. S. Cross, and M. Tsukada, Phys. Rev. B **66**, 214109 (2002).
[105]D. Drury, K. Yazawa, A. Zakutayev, B. Hanrahan, and G. Brennecka, Micromachines **13**, 887 (2022).
[106]H. Moriwake, A. Konishi, T. Ogawa, K. Fujimura, C. A. J. Fisher, A. Kuwabara, T. Shimizu, S. Yasui, and M. Itoh, Appl. Phys. Lett. **104**, 242909 (2014).
[107]G. Henkelman, B. P. Uberuaga, and H. Jonsson, J. Chem. Phys. **113**, 9901 (2000).
[108]S. Zhang, D. Holec, W. Y. Fu, C. J. Humphreys, and M. A. Moram, J. Appl. Phys. **114**, 133510 (2013).
[109]S. Yasuoka, T. Shimizu, A. Tateyama, M. Uehara, H. Yamada, M. Akiyama, Y. Hiranaga, Y. Cho, and H. Funakubo, J. Appl. Phys. **128**, 114103 (2020).
[110]F. Tasnadi, B. Alling, C. Hoglund, G. Wingqvist, J. Birch, L. Hultman, and I. A. Abrikosov, Phys. Rev. Lett. **104**, 137601 (2010).
[111]H. Momida and T. Oguchi, Appl. Phys. Express **11**, 041201 (2018).
[112]H. Moriwake, R. Yoko, A. Taguchi, T. Ogawa, C. A. J. Fisher, A. Kuwabara, Y. Sato, T. Shimizu, Y. Hamasaki, H. Takashima, and M. Itoh, APL Mater. **8**, 121102 (2020).
[113]D. Wang, P. Wang, M. He, J. Liu, S. Mondal, M. Hu, D. Wang, Y. Wu, T. Ma, and Z. Mi, Appl. Phys. Lett. **122**, 090601 (2023).
[114]J. Y. Yang, S. Y. Oh, M. J. Yeom, S. Kim, G. Lee, K. Lee, S. Kim, and G. Yoo, IEEE Electron Device Lett. **44**, 1260 (2023).
[115]J. Casamento, K. Nomoto, T. S. Nguyen, H. Lee, C. Savant, L. Li, A. Hickman, T. Maeda, J. Encomendero, V. Gund, A. Lal, J. C. M. Hwang, H. G. Xing, and D. Jena, in Proceedings of IEEE International Electron Devices Meeting (IEDM) (IEEE, San Francisco, C, 2022), pp.11.1.1–11.1.4.
[116]H. Zhou, D. Kwon, A. B. Sachid, Y. Liao, K. Chatterjee, A. J. Tan, A. K. Yadav, C. Hu, and S. Salahuddin, in *Proceedings of IEEE Symposium on VLSI Technology* (IEEE, Honolulu, HI, 2018), pp. 53–54.
[117]X. Liu, D. Wang, K. H. Kim, K. Katti, J. Zheng, P. Musavigharavi, J. Miao, E. A. Stach, R. H. Olsson III, and D. Jariwala, Nano Lett. **21**, 3753 (2021).

[118]K. Nomoto, B. Song, Z. Hu, M. Zhu, M. Qi, N. Kaneda, T. Mishima, T. Nakamura, D. Jena, and H. G. Xing, IEEE Electron Device Lett. **37**, 161 (2016).
[119]T. Maeda, T. Narita, H. Ueda, M. Kanechika, T. Uesugi, T. Kachi, T. Kimoto, M. Horita, and J. Suda, Appl. Phys. Lett. **115**, 142101 (2019).
[120]S. Rajan, H. Xing, S. DenBaars, U. K. Mishra, and D. Jena, Appl. Phys. Lett. **84**, 1591 (2004).
[121]J. Simon, V. Protasenko, C. Lian, H. Xing, and D. Jena, Science **327**, 60 (2010).
[122]S. Li, M. Ware, J. Wu, P. Minor, Z. Wang, Z. Wu, Y. Jiang, and G. J. Salamo, Appl. Phys. Lett. **101**, 122103 (2012).
[123]Izhar, M. M. Fiagbenu, P. Musavigharavi, X. Du, J. Leathersich, C. Moe, A. Kochhar, E. A. Stach, R. Vetury, and R. H. Olsson III, IEEE Electron Device Lett. **44**, 1196 (2023).
[124]S. Nam, W. Peng, P. Wang, D. Wang, Z. Mi, and A. Mortazawi, IEEE Microwave Wireless Technol. Lett. **33**, 803 (2023).
[125]J. P. B. Silva, R. Alcala, U. E. Avci, N. Barrett, L. Bégon-Lours, M. Borg, S. Byun, S. C. Chang, S. W. Cheong, D. H. Choe, J. Coignus, V. Deshpande, A. Dimoulas, C. Dubourdieu, I. Fina, H. Funakubo, L. Grenouillet, A. Gruverman, J. Heo, M. Hoffmann, H. Alex Hsain, F. T. Huang, C. S. Hwang, J. Íñiguez, J. L. Jones, I. V. Karpov, A. Kersch, T. Kwon, S. Lancaster, M. Lederer, Y. Lee, P. D. Lomenzo, L. W. Martin, S. Martin, S. Migita, T. Mikolajick, B. Noheda, M. Hyuk Park, K. M. Rabe, S. Salahuddin, F. Sánchez, K. Seidel, T. Shimizu, T. Shiraishi, S. Slesazeck, A. Toriumi, H. Uchida, B. Vilquin, X. Xu, K. Hee Ye, and U. Schroeder, APL Mater. **11**, 089201 (2023).
[126]M. Si, Y. Hu, Z. Lin, X. Sun, A. Charnas, D. Zheng, X. Lyu, H. Wang, K. Cho, and P. D. Ye, Nano Lett. **21**, 500 (2021).
[127]Z. Lin, M. Si, V. Askarpour, C. Niu, A. Charnas, Z. Shang, Y. Zhang, Y. Hu, Z. Zhang, P. Y. Liao, K. Cho, H. Wang, M. Lundstrom, J. Maassen, and P. D. Ye, ACS Nano **16**, 21536 (2022).
[128]X. Liu, J. Ting, Y. He, M. Mercy, A. Fiagbenu, J. Zheng, D. Wang, J. Frost, P. Musavigharavi, G. Esteves, K. Kisslinger, S. B. Anantharaman, E. A. Stach, R. H. Olsson III, and D. Jariwala, Nano Lett. **22**, 7690 (2022).
[129]I. Ham, Y. Jeong, S. J. Baik, and M. Kang, Electronics **10**, 38 (2020).